NeuroImage 56 (2011) 1222–1234

Contents lists available at ScienceDirect

NeuroImage

journal homepage: www.elsevier.com/locate/ynimg

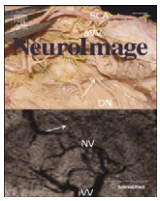

Characterizing dynamic functional connectivity in the resting brain using variable parameter regression and Kalman filtering approaches

Jin Kang [a,1], Liang Wang [b,1], Chaogan Yan [a], Jinhui Wang [a], Xia Liang [a], Yong He [a,*]

[a] State Key Laboratory of Cognitive Neuroscience and Learning, Beijing Normal University, Beijing, China
[b] Department of Psychiatry, University of British Columbia, Vancouver, British Columbia, Canada

ARTICLE INFO

Article history:
Received 5 November 2010
Revised 5 March 2011
Accepted 9 March 2011
Available online 21 March 2011

Keywords:
Resting-state fMRI
Connectivity
Networks
Dynamics
Default mode
Spontaneous brain activity

ABSTRACT

The cognitive activity of the human brain benefits from the functional connectivity of multiple brain regions that form specific, functional brain networks. Recent studies have indicated that the relationship between brain regions can be investigated by examining the temporal interaction (known as functional connectivity) of spontaneous blood oxygen level-dependent (BOLD) signals derived from resting-state functional MRI. Most of these studies plausibly assumed that inter-regional interactions were temporally stationary. However, little is known about the dynamic characteristics of resting-state functional connectivity (RSFC). In this study, we thoroughly examined this question within and between multiple functional brain networks. Twenty-two healthy subjects were scanned in a resting state. Several of the RSFC networks observed, including the default-mode, motor, attention, memory, auditory, visual, language and subcortical networks, were first identified using a conventional voxel-wise correlation analysis with predefined region of interests (ROIs). Then, a variable parameter regression model combined with the Kalman filtering method was employed to detect the dynamic interactions between each ROI and all other brain voxels within each of the RSFC maps extracted above. Experimental results revealed that the functional interactions within each RSFC map showed time-varying properties, and that approximately 10–20% of the voxels within each RSFC map showed significant functional connectivity to each ROI during the scanning session. This dynamic pattern was also observed for the interactions between different functional networks. In addition, the spatial pattern of dynamic connectivity maps obtained from neighboring time points had a high similarity. Overall, this study provides insights into the dynamic properties of resting-state functional networks.

© 2011 Elsevier Inc. All rights reserved.

Introduction

Spontaneous neuronal activity of the human brain consumes one-fifth of the body's energy and plays an important role in reflecting the brain's intrinsic mental state and human behavior (Fox and Raichle, 2007). Spontaneous blood oxygen level-dependent (BOLD) signals in resting-state functional MRI (fMRI) relate to spontaneous neuronal activity (Shmuel and Leopold, 2008). The investigation of spontaneous BOLD activity in the human brain has generated a new avenue of neuroimaging research.

Using resting-state fMRI, Biswal et al. (1995) first showed that spontaneous BOLD fluctuations between the bilateral somatomotor cortices were highly correlative in the absence of motor performance. Many neuroimaging studies have consistently identified functionally integrated maps in various brain networks, such as the motor (Lowe et al., 1998), visual (Hampson et al., 2002), auditory (Cordes et al., 2001), attention (Fox et al., 2006) and default-mode networks (Greicius et al., 2003). These functional brain networks have a high reproducibility across subjects (Damoiseaux et al., 2006; Buckner et al., 2009; He et al., 2009), time (Shehzad et al., 2009; Zuo et al., 2010) and research sites (Long et al., 2008; Biswal et al., 2010). Of note, one important and popular method for identifying these brain systems was a seed-based correlation analysis (Biswal et al., 1995). Using this method, researchers usually extract a representative BOLD time series from a given seed region based on previous anatomical or functional studies and calculate temporal correlations between this signal and the time series from all other voxels across the brain. The basis of this method is the assumption that the inter-regional correlations remain temporally stationary during an entire scan. However, many functional imaging studies have provided increasing evidence for a dynamic interaction between different brain regions during both the performance of tasks and a resting state. For example, several fMRI studies have demonstrated that the interdependence between brain regions shows temporal fluctuations during the post-stimulus time of a trial (Liu et al., 1999), across trials with task switches (Buchel and Friston, 1998; Kellya et al., 2007) and during learning (Lewis et al., 2009). Using a high time resolution measurement, Valencia et al. (2008) reported that an inter-regional functional integration on a large-scale level showed dynamic behavior

* Corresponding author. Fax: +86 1058802036.
E-mail address: yong.he@bnu.edu.cn (Y. He).
[1] These authors contributed equally to this work.

1053-8119/$ – see front matter © 2011 Elsevier Inc. All rights reserved.
doi:10.1016/j.neuroimage.2011.03.033

across events. These dynamic associations fit well with the notion that large-scale neural networks show the ability to perform dynamic reconfigurations that adapt to external experimental tasks (Bressler, 1995), which play vital roles in various cognitive activities (Kelly et al., 2008). Therefore, we also thought it interesting to explore the dynamic functional connectivity patterns in a resting state. A resting-state fMRI study in rats demonstrated that spontaneous BOLD activity in the cerebral cortex presented a dynamic propagation process from the somatosensory cortex to the primary motor cortex (Majeed et al., 2009), implying the appearance of dynamic connectivity in the task-free or resting state. A recent study in humans utilized a time–frequency analysis to observe dynamic associations between the default-mode and attention networks across time (Chang and Glover, 2010). However, the dynamic relationship between brain regions in a resting state was investigated rarely. In this study, we introduced a method, the variable parameter regression (VPR) combined with Kalman filtering approach (Klaman, 1960; Garbade, 1977; Digalakis and Rohlicek, 1993), to detect whether and how such fluctuating connectivity appears within and between multiple functional brain networks.

In the present study, we first applied the VPR analysis and Kalman filtering method to a simulated data to detect the sensitivity and the validity of the method. Then we applied the method to a real resting-state fMRI dataset to examine dynamic functional connectivity patterns in eight brain functional networks, including the motor, visual, auditory, attention, memory, subcortical, language and default-mode networks. To do this, we first selected eight seed regions to create specific functional networks, based on the coordinates reported in previous studies [motor (Jiang et al., 2004), visual (Lowe et al., 1998), auditory (Rademacher et al., 2001), attention (Fox et al., 2005), memory (Vincent et al., 2006), subcortical (Zou et al., 2009b), language (Xiang et al., 2010) and default-mode networks (Fox et al., 2005)] (for details, see Materials and methods). We examined the dynamics of functional connectivity within and between the brain networks detailed above by combining the VPR and Kalman filtering approaches (Klaman, 1960; Garbade, 1977; Digalakis and Rohlicek, 1993). On the basis of these previous studies, we hypothesized that the functional interactions within and between the brain networks would change dynamically across time.

Materials and methods

Participants

Twenty-two healthy right-handed college students (11 females, 20.1 ± 1.67 years, ranging from 17 to 24 years) participated in this study. They were recruited using advertisements on the campus of the Beijing Normal University. They had no history of neurological or psychiatric disorders. Written informed consent was obtained from each participant, and this study was approved by the Institutional Review Board of Beijing Normal University Imaging Center for Brain Research. Of note, the data was selected from a large sample resting-state fMRI dataset, which has been publicly released in the "1000 Functional Connectomes" Project (http://www.nitrc.org/projects/fcon_1000/).

Image acquisition

The resting-state fMRI data were acquired using a SIEMENS TRIO 3-Tesla scanner in the Imaging Center for Brain Research, the Beijing Normal University. During data acquisition, the participants were supine with the head fixed by straps and were instructed to keep awake with their eyes closed. The functional images were obtained using an echo-planar imaging sequence with the following parameters: 33 axial slices, time repetition (TR) = 2000 ms, time echo (TE) = 30 ms, thickness/gap = 3/0.6 mm, flip angle (FA) = 90°, field-of-view (FOV) = 200 × 200 mm^2, in-plane resolution = 64 × 64. The scan lasted 8 min. After scanning, all participants reported that they had not fallen asleep during the scan. In addition, a T1-weighted sagittal three-dimensional structural image was acquired using a magnetization-prepared rapid gradient echo (MPRAGE) sequence: 128 slices, TR = 2530 ms, TE = 3.39 ms, slice thickness = 1.33 mm, FA = 7°, FOV = 256 × 256 mm^2, and in-plane resolution = 256 × 192.

fMRI data preprocessing

Data preprocessing was performed using the SPM5 software package (http://www.fil.ion.ucl.ac.uk/spm). The first 10 volumes of each subject were discarded to allow for the stabilization of the MR signals. The preprocessing steps included a slice-timing correction on the time interval across slices, a head motion correction with a 6 parameter affine transformation, spatial normalization to MNI coordinate space using an optimum 12-parameter affine transformation and nonlinear deformations (Ashburner and Friston, 1999) followed by resampling to 3-mm isotropic voxels, spatial smoothing with a 4-mm FWHM Gaussian kernel, and detrend and temporal band-pass filtering (0.01–0.1 Hz).

Generation of static resting-state functional connectivity maps

In this study, we first examined the functional connectivity patterns of each brain network using a seed-based correlation analysis, referred to as static resting-state functional connectivity (S-RSFC). Briefly, the region of interest (ROI) related to each brain network was first obtained from previous studies (see Table 1 for detailed information). We then created an ROI with 6-mm radius spheres at the center of the coordinates shown in Table 1. In this study, we evaluated the effects of different choices of radius size on the results. We re-created spherical ROIs with a radius size of 8-mm, 6-mm and 4-mm and then extracted the time series from these ROIs and found these time series showed high similarities (data not shown), suggesting that different radius sizes did not significantly change our results. The BOLD time courses within each ROI were extracted and averaged over all of the voxels. The resulting BOLD signal was centered and normalized to a mean of zero and a variance of one. The S-RSFC maps were generated by Pearson's correlation between the seed-based time course and each voxel with the global mean signal, the white matter signal, the cerebrospinal fluid signal and six head motion parameters as covariates. The range of each S-RSFC map was constrained within a predefined gray matter mask generated by setting the probability value greater than 0.25 of the gray matter probabilistic map in the standard space obtained from SPM 5. These maps were tested using a one-tailed one sample *t*-test (confining the significantly positive correlation) and corrected for multiple comparisons ($p<0.05$ corrected; cluster volume > 54 mm^3; FWHM = 4 mm) based on the Monte Carlo program implemented in AFNI (http://afni.nimh.nih.gov/afni). In this study, we focused on inter-regional positive correlations because the origin of negative correlations remains poorly understood (Fox et al., 2009; Murphy et al., 2009).

Variable parameter regression analysis

To describe the dynamic resting-state functional connectivity (D-RSFC) of brain regions (or voxels), we used a variable parameter regression method (Garbade, 1977), which is briefly described as follows:

$$y_t = x_t\beta_t + u_t, \quad t = 1,\ldots,T, \tag{1}$$

$$u_t \sim N\left(0,\sigma^2\right) \tag{2}$$

$$\text{and,} \quad \beta_t = \beta_{t-1} + p_t, \quad t = 2,\ldots,T, \tag{3}$$

$$p_t \sim N(0,\sigma^2 P) \tag{4}$$

Table 1
Definition of ROIs and relevant functional connectivity networks.

Abbr.	ROIs	MNI coordinates			Brain networks	Functionally connected regions to ROIs
		x	y	z		
PCC.L	Left posterior cingulate cortex	−5	−52	41	Default mode (Fox et al., 2005)	Medial prefrontal cortex (BA9/10/11), lateral temporal and parietal cortical regions
FEF.R	Right frontal eye field	25	−16	54	Attention (Fox et al., 2005)	Inferior parietal lobe (BA 40), superior parietal gyrus (BA 4/6) and postcentral gyrus
HF.L	Left hippocampal formation	−21	−25	−18	Memory (Vincent et al., 2006)	Right hippocampus, posterior cingulate cortex, medial prefrontal cortex (BA9/10/11), lateral temporal and parietal cortical regions
PMC.L	Left primary motor cortex	−43	−28	53	Motor (Jiang et al., 2004)	Supplement motor cortex (SMA, Brodmann Area [BA] 6), superior cerebellum (SCb) and primary motor cortex (M1, BA 4)
PAC.L	Left primary auditory cortex	−42	−22	6	Auditory (Rademacher et al., 2001)	Superior temporal gyrus, supplemental motor area and insula (BA 41/48)
CF.L	Left calcarine fissure	−10	−78	7	Visual (Lowe et al., 1998)	Calcarine sulcus, lingual gyrus (BA 17) and cuneus (BA 18)
POP.L	Left pars opercularis	−50	13	18	Language (Xiang et al., 2010)	Inferior frontal gyrus (BA 44/45/48), inferior parietal lobule (BA 40), supramarginal gyrus (SMG) and precentral gyrus (BA 6)
TH.R	Right thalamus (mediodorsal nuclei)	6	−16	9	Subcortical (Zou et al., 2009b)	Cingulate cortex (BA 24/23/26), insula, precuneus, putamen and amygdala

The Talairach coordinates of the ROIs reported in these studies are translated into MNI coordinates using tal2mni program (http://eeg.sourceforge.net/doc_m2html/bioelectromagnetism/tal2mni.html). The last column represents brain regions showing significant functional connectivity with the ROIs. MNI = Montreal Neurological Institute; Abbr. = abbreviation.

where y_t and x_t are two values of the time series of voxels y and x at time t, respectively; β_t is an estimated coefficient that reflects the functional connectivity between the two voxels at time t; T denotes the number of the scan. The stochastic vector u_t is normally distributed with a mean of zero and a variance of σ^2 and p_t with a mean of zero and a variance of $\sigma^2 P$. There were no correlations between the two stochastic vectors. Apparently, variable parameter regression becomes a linear regression in the case of $P=0$. Practically, P was usually close to zero when the following steps were used.

The parameter estimation was conducted using the Kalman filtering model to produce an optimal solution (Garbade, 1977). We defined $\hat{\beta}_t(t)$ as an estimate of β_t at time t and let $\sigma^2 S_t$ and $\sigma^2 R_t$ be the estimated covariance matrix of $\hat{\beta}_t(t)$ and $\hat{\beta}_t(t-1)$, respectively. First, we obtained a prediction that updated $\hat{\beta}_{t-1}(t-1)$ and its covariance matrix for the passage of time from $t-1$ to t:

$$\hat{\beta}_t(t-1) = \hat{\beta}_{t-1}(t-1) \tag{5}$$

$$R_t = S_{t-1} + P. \tag{6}$$

Based on Eqs. (5) and (6), we could estimate the next time state from the current state. Second, the estimated $\hat{\beta}_t(t-1)$ and its covariance R_t were updated to $\hat{\beta}_t(t)$ and S_t by adding new information contained from the measurement y_t:

$$\hat{\beta}_t(t) = \hat{\beta}_t(t-1) + K_t e_t. \tag{7}$$

$$\text{Here}, e_t = y_t - x_t\,\hat{\beta}_t(t-1)$$

$$\text{and}, K_t = R_t x_t' E_t^{-1}$$

$$\text{and}, E_t = x_t R_t x_t' + 1. \tag{8}$$

$$S_t = R_t - K_t x_t R_t \tag{9}$$

where e_t is the residual measurement at time t. It reflects the residual of relationship of the signals y and the estimated y and it is expected to be close to zero and obeys Gaussian distribution with variance $\sigma^2 E_t$. E_t can be obtained from the measurement residual equation. Because the estimates of $\hat{\beta}_t(t)$ were generally less reliable based on information before time t than later times, in the third step we constructed a smoothed estimate, $\hat{\beta}_t(T)$, and its covariance, V_T, by adding the latter information.

$$\hat{\beta}_t(T) = \hat{\beta}_t(t) + G_t\left[\hat{\beta}_{t+1}(T) - \hat{\beta}_t(t)\right] \tag{10}$$

$$\text{where}, G_t = S_t[S_t + P]^{-1}$$

$$V_t = S_t + G_t\left[V_{t+1} - R_{t+1}\right]G_t' \tag{11}$$

$$V_T = S_T. \tag{12}$$

From the equations above, $\hat{\beta}_t(T)$ was constant before and after smoothness when P was equal to zero. So far, we have assumed σ^2 and P are known. However, we can estimate the two parameters by the maximum likelihood shown in the next step. The log-likelihood function involving P and σ^2 is

$$L = -\frac{1}{2}\sum_{t=n+1}^{T} ln\left(\sigma^2 E_t\right) - \frac{1}{2}\sum_{t=n+1}^{T}\left\{\frac{e_t^2}{\sigma^2 E_t}\right\}. \tag{13}$$

For a given P, an estimate of σ^2 is available by the analytical maximization of Eq. (13):

$$\hat{\sigma}^2 = \sum_{t=n+1}^{T}\left\{\frac{e_t^2}{(T-n)E_t}\right\}. \tag{14}$$

The substituted log-likelihood function is then:

$$L^*(P) = -(T-n)\,ln\left(\hat{\sigma}\right) - \frac{1}{2}\sum_{t=n+1}^{T} ln(E_t). \tag{15}$$

Because both $\hat{\sigma}$ and E_t are implicit functions of P in terms of Eqs. (6) and (8), L^* becomes a complicated nonlinear function of P.

The estimator of time-related regression coefficients approximately fits to a standard normal distribution with a mean equal to $\hat{\beta}_t(T)$ and a standard deviation (SD) $\sigma V_T^{1/2}$. The 95% confidence intervals for the estimate extended above and below $2\sigma V_T^{1/2}$, i.e., $\hat{\beta}_t(T) \pm 2\sigma V_T^{1/2}$. Therefore, if the enclosed range did not cover zero at a time point, a rejection of the null hypothesis was indicated (i.e., no significant connectivity between the two signals) at the 5% significance level, suggesting the regression coefficient at time point t was significantly different from zero. If the range from $\hat{\beta}_t(T) - 2\sigma V_T^{1/2}$ to $\hat{\beta}_t(T) + 2\sigma V_T^{1/2}$ included a constant value except for zero over time, this suggests the estimated regression coefficient $\hat{\beta}_t(T)$ was stable over time. In this study, we applied the CAPTAIN Toolbox (http://www.es.lancs.ac.uk/cres/captain/) to estimate the parameters.

Simulated signal

In this study, we initially applied the combined VPR analysis and Kalman filtering method to simulated data. Two signals, x and y, were

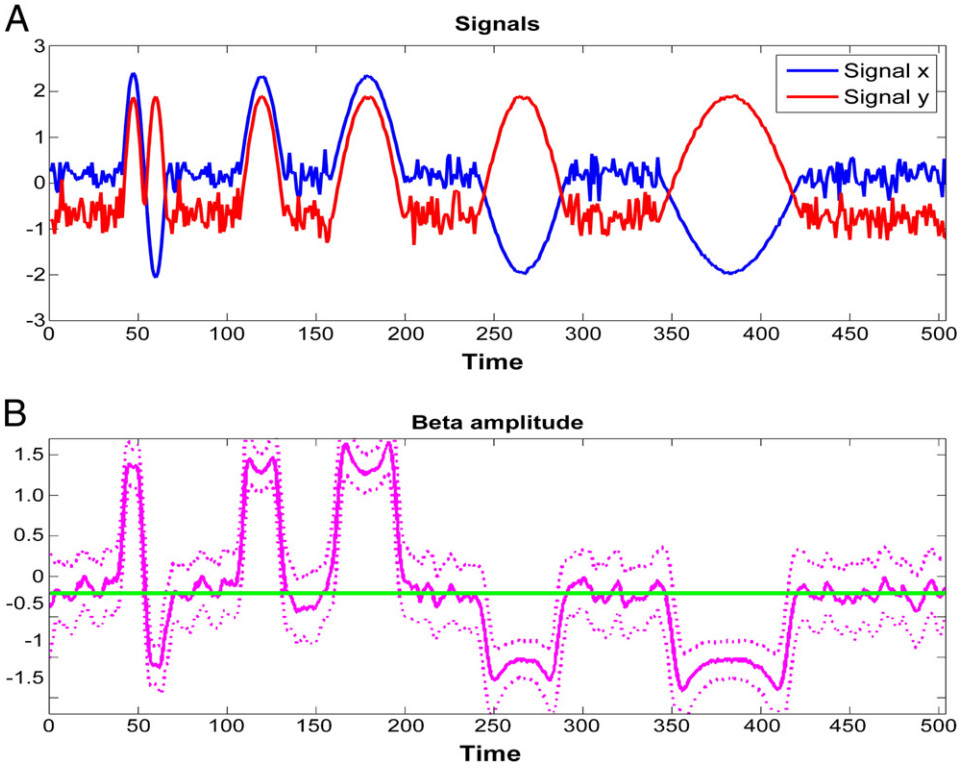

Fig. 1. The simulated data and dynamic interactions. (A) Signal x is composed of five sine parts, including a sinusoidal part and four half-sinusoidal parts, and six noise parts. The blue and red lines denote signals x and y, respectively. The two signals are normalized to a mean = 0 and a variance = 1. To be clearly represented, signal y is shifted down lightly. (B) Linear regression coefficient equivalent to Pearson's correlation coefficient between the two time series is shown as the green line and the dynamic regression coefficient is drawn as the pink line. The pink broken line indicates the standard errors.

generated (Fig. 1). Both the signals contained 504 time points, including a sinusoidal part and four half-sinusoidal parts and six noise parts. The noise parts met a normal distribution with mean 0 and variance 0.2 with 40, 40, 26, 41, 51 and 81 sample sizes, and the sinusoidal parts had a sinusoidal part with 26 time point and four half sinusoidal parts the same length as the noises from the last four parts. The sinusoidal parts of signals x and y were mixed with white noises with mean 0 and variance 0.02. For the signals *x* and *y*, the sine parts and noise parts were arranged alternatively. To be clearly represented, the signal y is shifted down lightly. The two signals were separately mean-centered and normalized before the application of the variable parameter regression analysis.

Generation of dynamic RSFC (D-RSFC) maps

D-RSFC maps were examined by using the VPR analysis and by computing the relationship between the time course of the ROI and any voxel within the S-RSFC maps over time. Of note, the D-RSFC maps were derived based on the same preprocessed data as that used to generate S-RSFC maps. We obtained the dynamic regression coefficient and its standard error to identify significant functional connectivity at any time point. The D-RSFC strength probability distribution maps were obtained by calculating the percentage of the number of time points where the coefficient was significantly different from zero. If the strength probability of one given voxel was equal to 1, that voxel always showed significant functional connectivity to the ROI across time.

Dynamic relationship between different brain networks

After examining the fluctuations within the resting-state networks, we investigated the dynamics of the relationship between resting-state networks across time. We first obtained a representative time series by averaging time series over those voxels strongly and stably connected to a ROI. Then, these resulting means of the time series were independently mean-centered and variance-normalized. Finally, we applied the combined VPR analysis and Kalman filtering method again to exploring the dynamic associations between these time series representing different brain networks.

Spatial similarity of the D-RSFC maps across time

We also examined the spatial similarity of the dynamic regression maps between different time points using Kendall's concordance coefficient (KCC) (Kendall, 1938)

$$W = \frac{\sum (R_i)^2 - n(\overline{R})^2}{\frac{1}{12}K^2\left(n^3 - n\right)}. \tag{16}$$

In this equation, W is a KCC value of a given brain network, ranging from 0 to 1; R_i is the sum rank of the ith voxel within the network and n is the number of voxels within the S-RSFC maps. $\overline{R} = ((n+1)K)/2$ is the mean of the R_i. K is the number of the brain volume in a scan session (here $K = 230$).

KCC quantifies the similarity of a network across time during a resting state. We transformed W into an χ^2 statistic with degrees of freedom of $n-1$ using Eq. (17) (Legendre, 2005). The KCC of one network of the group is an average of all of the subjects.

$$\chi^2 = K(n-1)W \tag{17}$$

Spatial similarity between S-RSFC and D-RSFC maps

The D-RSFC maps represent the dynamic functional connectivity patterns of brain regions across time, whereas the S-RSFC maps were stable with a focus on the general relationship across brain regions. We also explored the spatial similarity of S-RSFC and D-RSFC maps to reveal the intrinsic relationship of the combined VPR analysis and Kalman filtering method and linear regression analyses. For each ROI, the corresponding S-RSFC and D-RSFC maps at a given time point were transformed to columns of two vectors, and the correlation coefficient was measured between the two vectors. We repeated this process for each of the time points. As a result, the patterns of correlation coefficients were described as a function of time. The spatial similarity between the S-RSFC and D-RSFC maps was described as a percentage of the area of the curve (i.e., a function of time) occupying the maximum possible area of the curve (the correlation coefficient at each time point was equal to 1).

Results

Simulated data

We utilized two simulated signals to establish the validity of the VPR analysis. The signals, x and y, were simulated using the conjunction of the sine function and random white noises alternately (Fig. 1). The application of Pearson's correlation to the two signals revealed that their correlation was approximately equal to 0 (i.e., the green line in Fig. 1B). However, it's easy to imagine that the real correlation between both signals was dynamically changing over time, rather having simply no correlation. Using the combined VPR analysis and Kalman filtering method approach, a high correlation between the high consistent/reversed signals was estimated at close to 1 (i.e., positive correlation) or −1 (i.e., negative correlation) and displayed in the form of beta amplitudes. In contrast, the interaction of the signals located between the half-sine signals (i.e., random parts) shifted toward zero. These results suggest that this approach can capture temporal dynamic correlations between the two signals.

S-RSFC maps

Several functional subsystems in the resting brain were studied using a seed-based correlation analysis (Fig. 2). For each subsystem, voxels with significantly positive correlations to each ROI were identified using a one sample t-test ($p<0.05$, cluster-based correction). These functional subsystems are separately described in Table 1.

D-RSFC maps

We examined D-RSFC maps by combining the VPR and Kalman filtering methods. Each D-RSFC map was constrained by a mask created by the corresponding S-RSFC map. We then computed the time-varying regression coefficients between the ROIs and all of the voxels within the mask. Movies of time-varying functional connectivity within each brain network were provided in the supplemental materials. In the memory network, the hippocampus showed high correlations with the medial posterior cingulate cortex over the entire run, but the coefficients between this region and the medial prefrontal cortex had a large variation (Supplemental Movie 3). An analogous phenomenon was observed in the motor network, in which the motor-related ROI had high and stable correlations with homogenous regions across time but had large fluctuations in the inferior motor cortex (Supplement Movie 4). The detail of the dynamic connectivity patterns between the voxels and the relevant ROIs could be found in all eight movies. To examine whether different voxels in the S-RSFC map recruited various strengths connected to the ROI, we calculated the number of time points where dynamic regression coefficient was significantly different from zero. The percentage of the number of time points where the coefficient was significantly different from zero for a representative subject is shown in Fig. 3. Some voxels showed significant correlation with ROIs at all time points (depicted as a yellow color) but not for other voxels (depicted as a red color). These results suggested that different voxels with high correlation coefficients exhibited different dynamic correlation patterns or variant connectivity strengths.

To further examine the probability of distribution of the connectivity, we created a histogram of a set of thresholds with an increment of 0.1 (Fig. 4). Most of the voxels with relatively weak connections to the ROI fell under the probability of 0.5. There were, however, only 10–20% of the voxels with strong connectivity, indicated by a probability close to 1. The distribution trend of each network appeared as an approximate chi-square distribution, if one ignored the bar with a probability of 1. The percentage of voxels with a probability less than 0.5 accounted for about 75%. As a consequence, a small percentage of voxels fell into a probability range of 0.5–0.9. Notably, the percentage increased rapidly when the probability threshold reached around 1. This profile was observed across all of the subsystems. Moreover, the number of voxels with strong connectivity to each ROI was stable across time and subjects (Fig. 5).

The similarity of D-RSFC maps

We calculated the spatial similarity of the D-RSFC maps among all time points in terms of the KCC. In this sense, each image map was first converted to a spatial vector and all vectors from all time points were entered into the KCC analysis, to evaluate the spatial similarity of these image maps. For each network across all subjects, the KCC distribution map is shown in Fig. 6. The KCC of each network was located in the range of 0.25–0.4. Further statistical tests on the KCC revealed that the D-RSFC maps were significantly consistent ($p<0.001$). Moreover, the similarity of the D-RSFC and S-RSFC maps was in the range of 0.43–0.61 (Fig. 7). The trend of the similarity of the D-RSFC and S-RSFC maps was similar to that obtained from the KCC distribution specific to the D-RSFC maps (Fig. 6) except for the different scale.

Dynamic relationships between the RSFC networks

In addition to the investigations of the dynamic connectivity within brain systems, we applied the combined VPR analysis and Kalman filtering method to exploring the time-varying relationship between the different brain functional networks. The mean linear correlation coefficients between each pair of networks and the standard deviations are shown in Fig. 8. We found that the default mode network was negatively correlated with the attention, motor, auditory, visual and language networks and positively correlated with the memory and subcortical networks. These findings are consistent with previous resting-state fMRI studies using an S-RSFC analysis (Greicius et al., 2003; Fox et al., 2005; Fransson, 2005; Wang et al., 2006; Uddin et al., 2009). For example, the default mode network potentially contributed to memory functions (Vincent et al., 2006), implying that both the default mode and memory networks may share brain regions.

Fig. 2. S-RSFC maps. The positive correlation maps of the default-mode, attention, memory, motor, auditory, visual, language and subcortical networks during the resting state. A group correlation map of each network was created using a one sample t-test, ($p<0.05$, corrected). The green circle and pink arrow of each map show the location of the ROI with the relevant MNI coordinates.

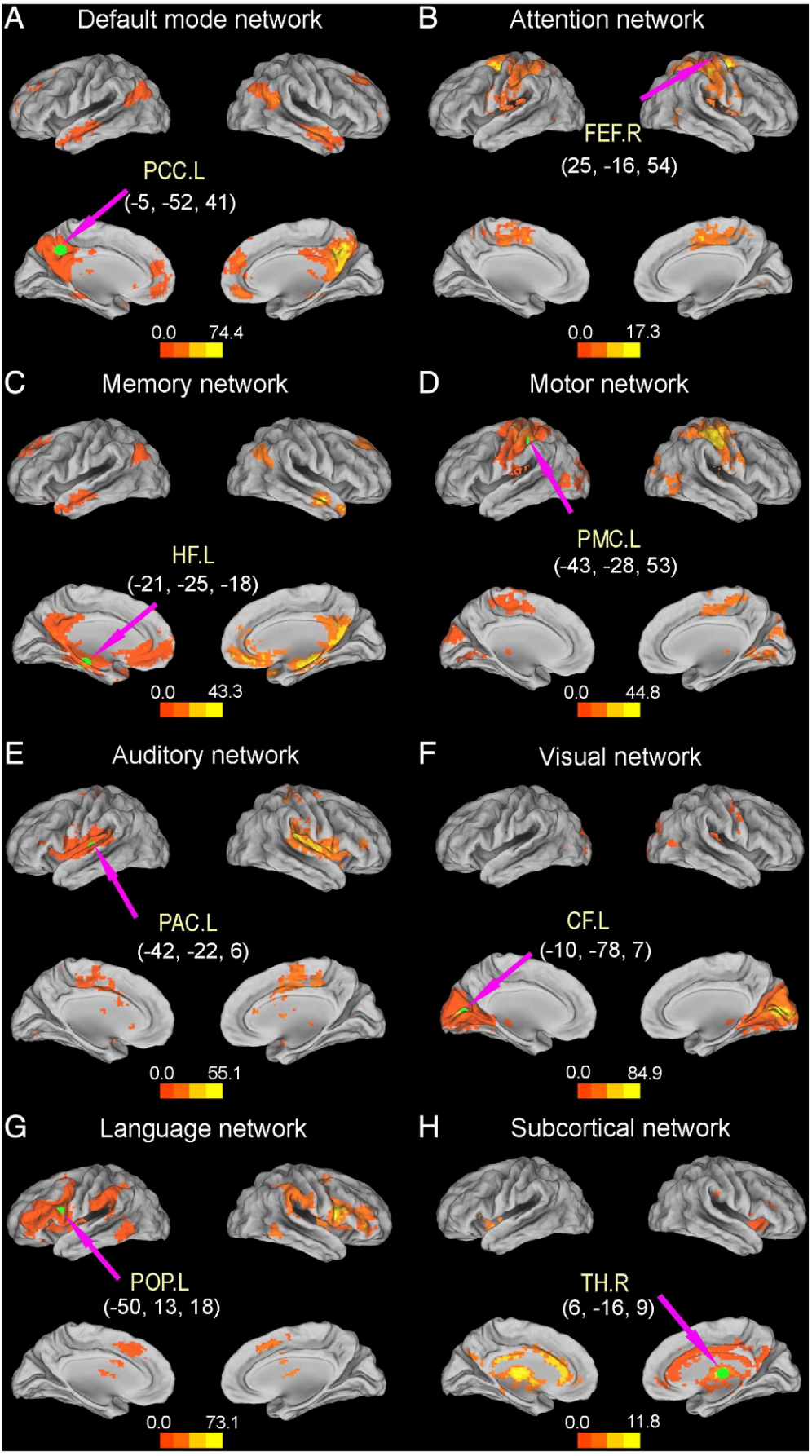
A
Default mode network
PCC.L
(-5, -52, 41)
0.0 74.4
B
Attention network
FEF.R
(25, -16, 54)
0.0 17.3
C
Memory network
HF.L
(-21, -25, -18)
0.0 43.3
D
Motor network
PMC.L
(-43, -28, 53)
0.0 44.8
E
Auditory network
PAC.L
(-42, -22, 6)
0.0 55.1
F
Visual network
CF.L
(-10, -78, 7)
0.0 84.9
G
Language network
POP.L
(-50, 13, 18)
0.0 73.1
H
Subcortical network
TH.R
(6, -16, 9)
0.0 11.8

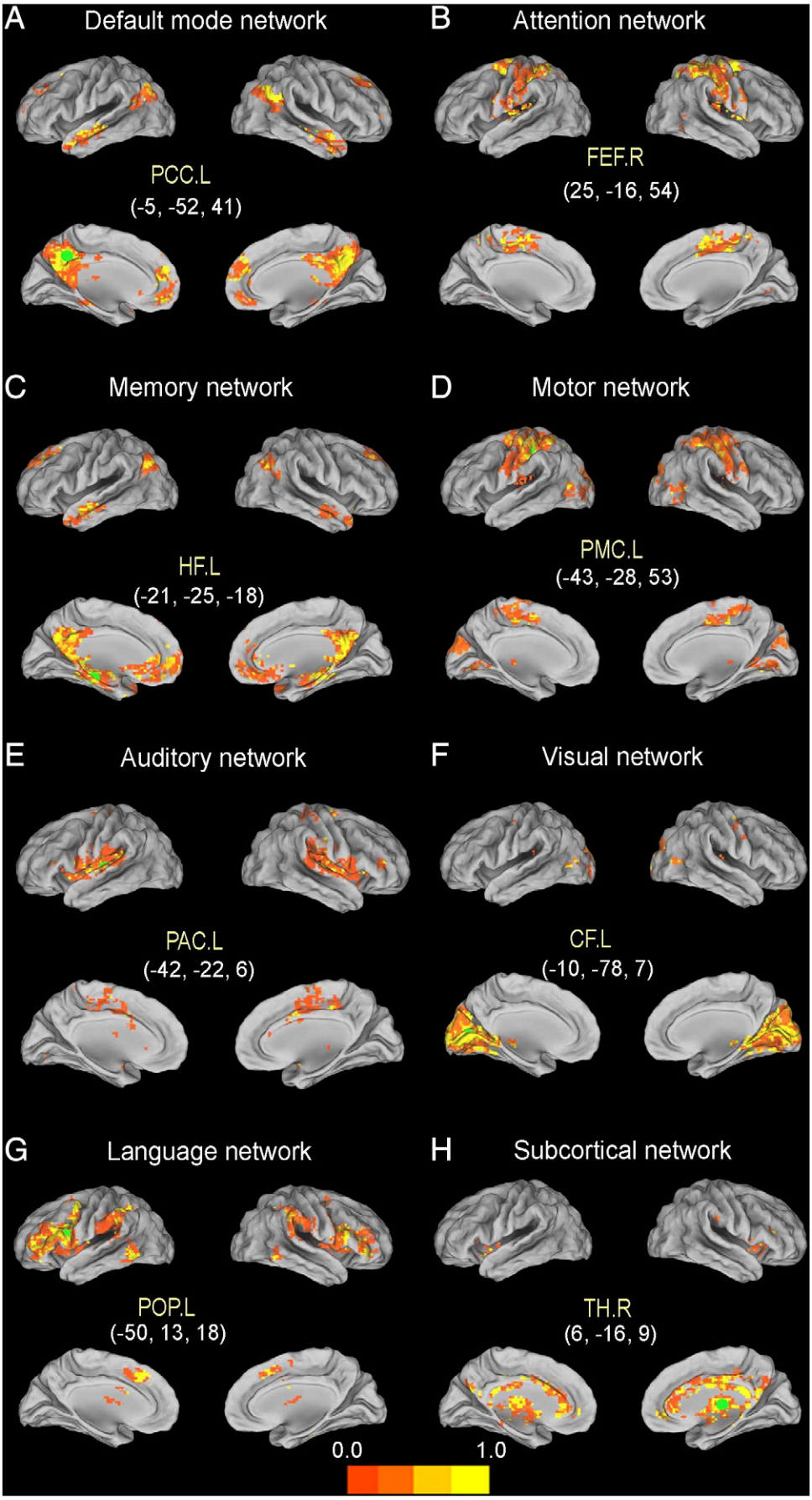
A
Default mode network
PCC.L
(-5, -52, 41)
B
Attention network
FEF.R
(25, -16, 54)
C
Memory network
HF.L
(-21, -25, -18)
D
Motor network
PMC.L
(-43, -28, 53)
E
Auditory network
PAC.L
(-42, -22, 6)
F
Visual network
CF.L
(-10, -78, 7)
G
Language network
POP.L
(-50, 13, 18)
H
Subcortical network
TH.R
(6, -16, 9)
0.0
1.0

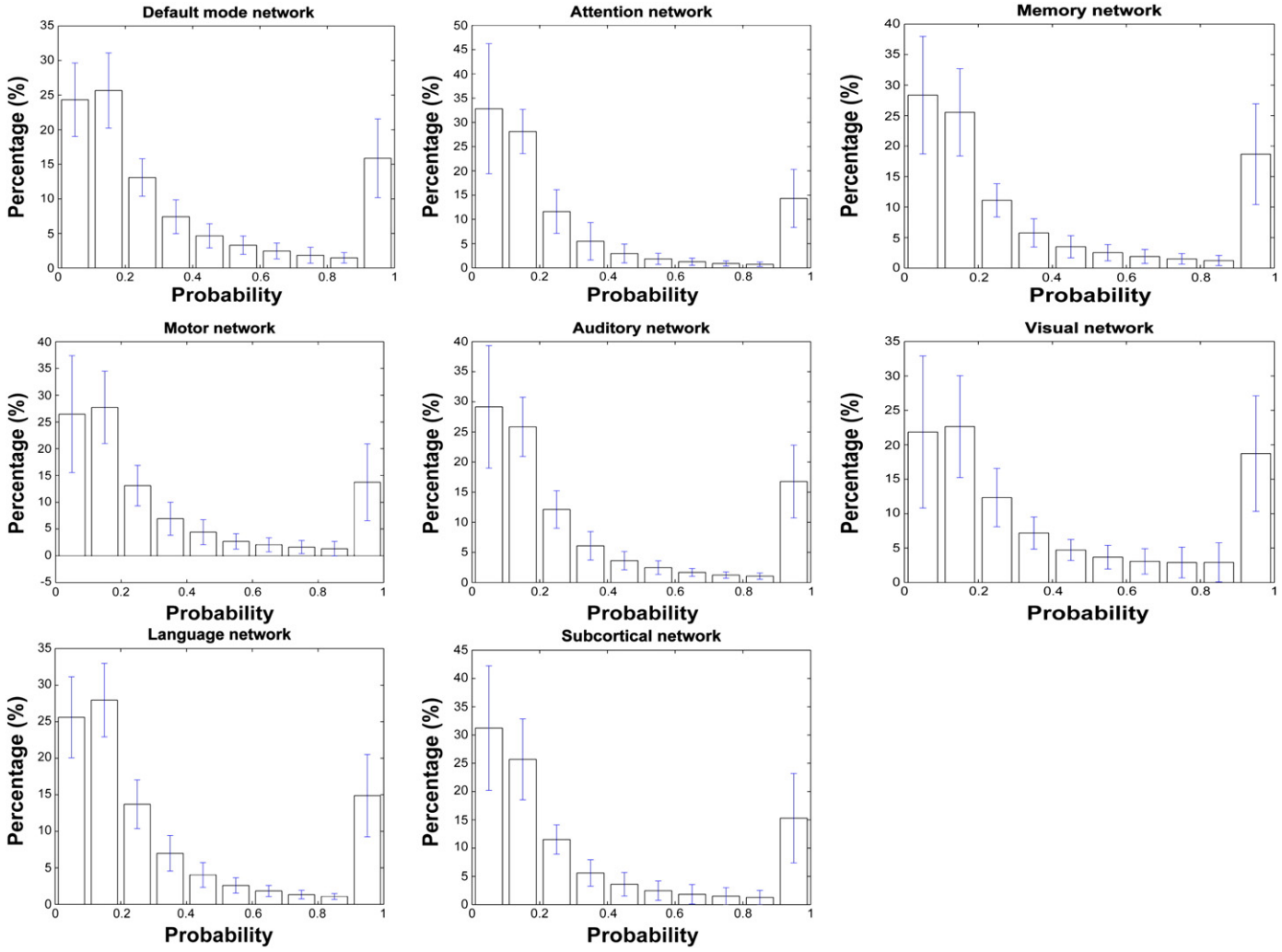

Fig. 4. Percentage of connectivity strength probability. The percentage of connectivity strength of each network is shown as an interval of 0.1. The probability means the number of time points at which regression coefficient was significantly different from zero, divided by the total number of time points (here, the value was 230). There was only a 10–20 percent strong connection in each of the eight systems. The error bars correspond to the standard error of the mean.

Discussion

In this study, we investigated a set of time-varying functional networks using a resting-state fMRI by combining the VPR analysis and the Kalman filtering model. The inter-regional interactions within and between these networks showed dynamic fluctuations over time, though there were few voxels with stable and strong connectivity with the predefined ROIs within each network.

Coherent fluctuations across regions have been previously examined using various methods, such as the linear correlation analysis and the independent component analysis. These methods predominantly investigated global properties over the whole scan time and provided that resting-state functional connectivity was static over time. An increasing number of studies have demonstrated that these resting-state functional networks are not only related to physiological activity but also consistent with the activation maps of goal-oriented tasks (Friston and Buchel, 2000; Lowe et al., 2000; Hampson et al., 2002; Jiang et al., 2004). Nonetheless, these resting state networks (RSNs) are slightly discrepant across different studies (Lowe et al., 1998; Cordes et al., 2000; Damoiseaux et al., 2006; Vincent et al., 2006). This diversity may be accounted for by differences in arousal and sleep levels (Fukunaga et al., 2006), emotional state (Harrison et al., 2008) and the dynamics of RSNs across time (Butts, 2009). These factors have been sufficiently discussed except for dynamics. Notably, the dynamic factor has been examined in a recent study using a time–frequency analysis (Chang and Glover, 2010). In the current study, the application of a novel method revealed dynamic functional connectivity both within and between multiple cognitive networks, which may contribute to the understanding of neuronal dynamics in a resting state as provided in a previous study (Haughton and Biswal, 1998).

Simulation data was first used to demonstrate the validity of the combined VPR analysis and Kalman filtering method (Fig. 1). For a comparison purpose, we also applied a sliding windows correlation method to the simulation data (Fig. S2). We found that our method exhibited better performance than sliding windows correlations in noise suppression and accurate estimation within the intervals between noise and sine parts. For the sliding windows correlations, we found the smaller the window size is, the more detailed the sliding correlation distribution will be, and the more noise effects. In contrast, the larger the window size is, the less accurately estimated value in the range from noise parts to sine parts will be. These results were compatible with a recent event-related potentials study showing

Fig. 3. The probability distribution of D-RSFC strength. The strength probability distribution maps of the default-mode, attention, memory, motor, auditory, visual, language and subcortical networks during the resting state. The green circle of each map shows the coordinates of the ROI. The different color-coded voxels in each network indicate different connectivity strengths with the ROI.

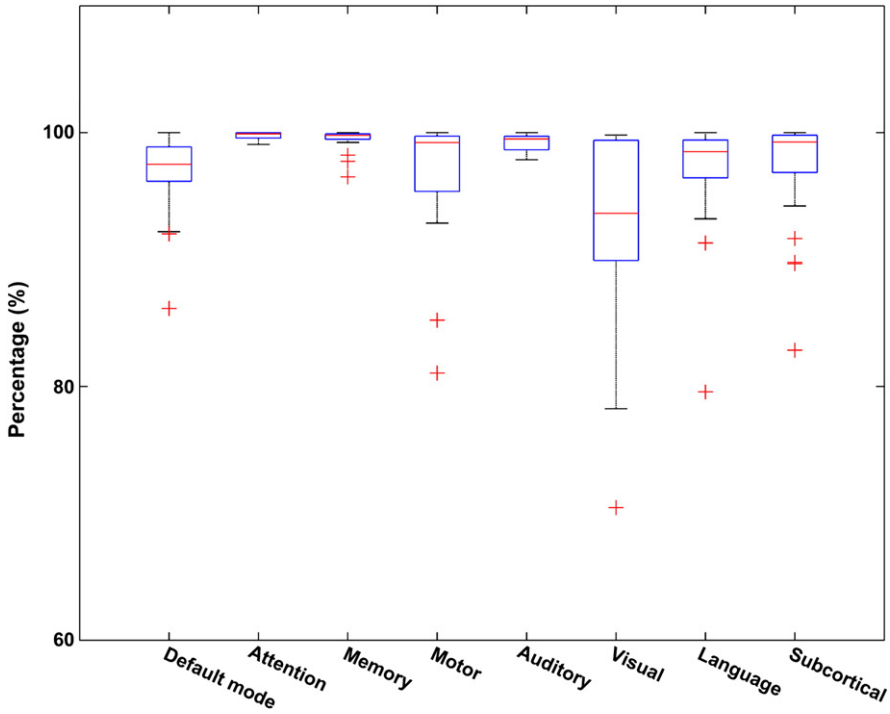

Fig. 5. Stability of strong functional connectivity. This boxplot shows median, interquartile, and range for the percentages of the group of subjects. The stability percentage of voxels that have strong connectivity with the ROIs was almost 100%.

better performances in a combined VPR analysis and Kalman filtering method than the sliding window averaging (Vedel-Larsen et al., 2010).

The observed dynamic coefficient reflected in Fig. 4 suggests that the traditional linear measurement may not entirely reflect the intrinsic interactions between brain regions, particularly those regions linked by discrepant anatomical structures. The stable and varying functional connectivity may contribute to the understanding of the relationship between brain structural and functional connectivity that structures the connectivity to provide the foundation for high-level functional connectivity. However, functional connectivity may just reflect structural restrictions to a certain extent (Damoiseaux and Greicius, 2009; Honey et al., 2009). To compare static linear coefficients and dynamical strength probabilities, we presented a scatter plot showing the static linear correlations (the values were set to absolute value) against the dynamical strength probabilities within the default mode network of a representative subject. There was a significant association between static and dynamic connections ($r=0.618$, $p<0.0005$, Fig. S1). This result indicates that the traditional seed-based correlations can partly reflect dynamic correlations (at a long time scale), though the dynamic correlations can capture the instantaneous relationship between two signals. Consequently, we speculate that those 10–20% of the voxels in the S-RSFC maps with a high connection probability close to 1 (reflecting strong connectivity) may be directly connected to prior ROIs by a number of white matter fibers, but other voxels with a low connection probability may be recruited indirectly or have no anatomical connectivity among them. Specifically, we found that bilateral homogenous networks, such as the attention, auditory and language networks, manifested a strong functional connectivity (Fig. 3) that are implemented by the corpus callosum connecting the left and right hemispheres (Johnston et al., 2008). The default mode network, with high connectivity between the posterior cingulate and medial prefrontal cortex, is connected by the superior longitudinal fasciculus and cingulate fiber tracts (Johnston et al., 2008; Greicius et al., 2009). All of these findings suggest that high probabilistic connections are related to anatomical connectivity. Recent studies have demonstrated that both static and dynamic cerebral blood flow characteristics exist in a single scan (Zou et al., 2009a), which may provide the basis of the coexistence of static and dynamic components in functional connectivity. Given the previous evidence and a hierarchy of processing frames at different temporal scales during sensory input (Kiebel et al., 2008), we speculate that functional connectivity between regions could be concurrently categorized into stable and dynamic components. The dissociated properties may correspond to a hierarchical conception; the bottom layer connections to central regions, as the backbone of a functional system related to anatomical connections, are robust and stable over time, but top layer connections, reflecting functional connections, are susceptible to external stimuli and easily modulated over time by other sources, such as levels of attention and mind-wandering. However, this speculation needs to be examined in future studies.

In addition, the current study reported an interesting finding that the D-RSFC maps exhibited high spatial similarity over time. This phenomenon was consistently observed in each functional network of each participant and could not be accounted for by potential acquisition artifacts. The values of the KCC of the visual and default-mode networks were larger than the others. Consistent with our finding, Damoiseaux et al. (2006) reported that the visual and default-mode networks exhibit a relatively high mean percentage of BOLD signal changes and a low variation around this mean across multiple subjects. In addition, Zuo et al. (2010) found that the most reliable resting-state networks were associated with attention selection and encoding, including primary visual perception and the default-mode network. The consistency across studies suggests that the visual and default-mode networks are more reliable and sustainable over time within subjects and between subjects. Notably, the co-appearance of both variability and persistence indicates that dynamic fluctuations in the RSFC maps have high continuity over time, implying the robustness of cognitive regions regardless of the appearance of cognitive tasks (Friston and Buchel, 2000; Achim and Lepage, 2005;

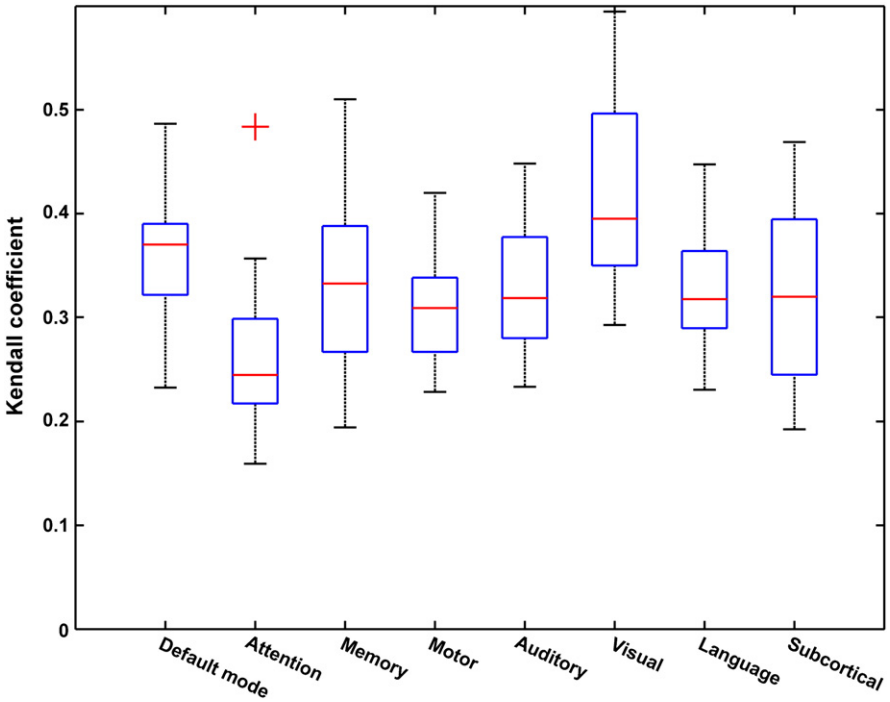

Fig. 6. Spatial similarity of the D-RSFC maps across time. The KCC of each network was mostly located in an interval from 0.25 to 0.4. Further statistical evaluation revealed that the D-RSFC maps were consistent (i.e., the relationship between voxels within the human brain was stable) across time ($p<0.001$). This boxplot shows median, interquartile, and range for the Kendall coefficients of the group of subjects.

Tian et al., 2007). This phenomenon is consistent with the previous notion that many systems have stable statistical properties at the global level but are more dynamic at the microscopic level (Gautreau et al., 2009).

Selective attention and goal-directed behavior are generally associated with increased activity in the task-positive networks and suppressed activity in task-negative networks (Cabeza et al., 2000; Simpson et al., 2000, 2001; Corbetta et al., 2002; Corbetta and Shulman, 2002; McKiernan et al., 2003). In contrast, stimulus-independent thoughts are associated with increased activity in task-negative networks and a trend toward decreased activity in task-positive networks (McGuire et al., 1996). Moreover, this negative correlation between the default-mode network and the attention network has been depicted by Fox et al. (2005). Consistent with these studies, we also observed that the default-mode network was anti-correlated with the motor, language and auditory networks. Although the anti-correlation changed over time because of the possible changes in states (e.g., arousal and noises) (Chang and Glover, 2010), a detailed mechanism remains unclear. Future studies will be helpful in clarifying this issue.

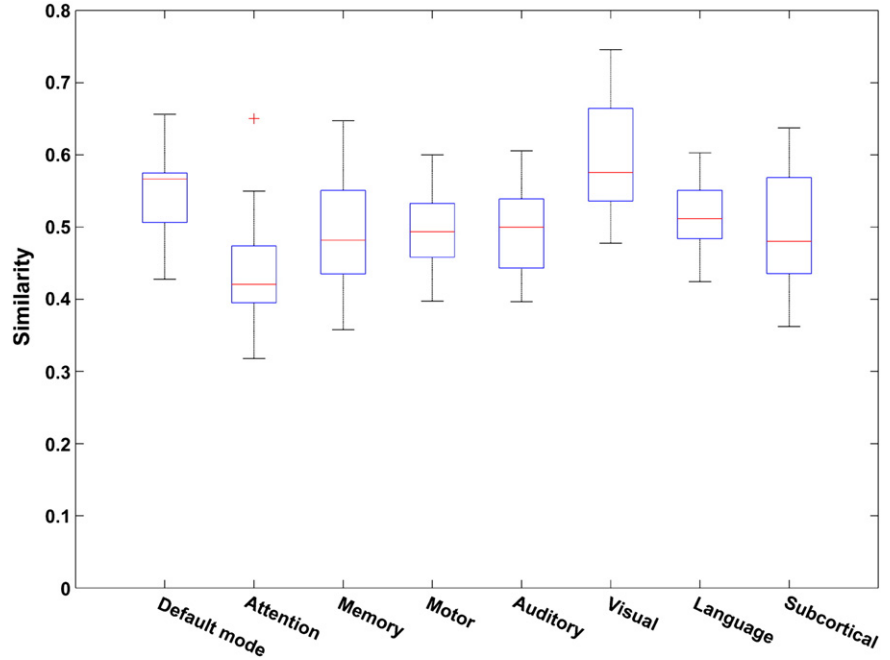

Fig. 7. Spatial similarity between the D-RSFC and S-RSFC maps. The similarity of D-RSFC maps and S-RSFC maps ranged from 0.43 to 0.61. This boxplot shows median, interquartile, and range for the spatial similarities of the group of subjects.

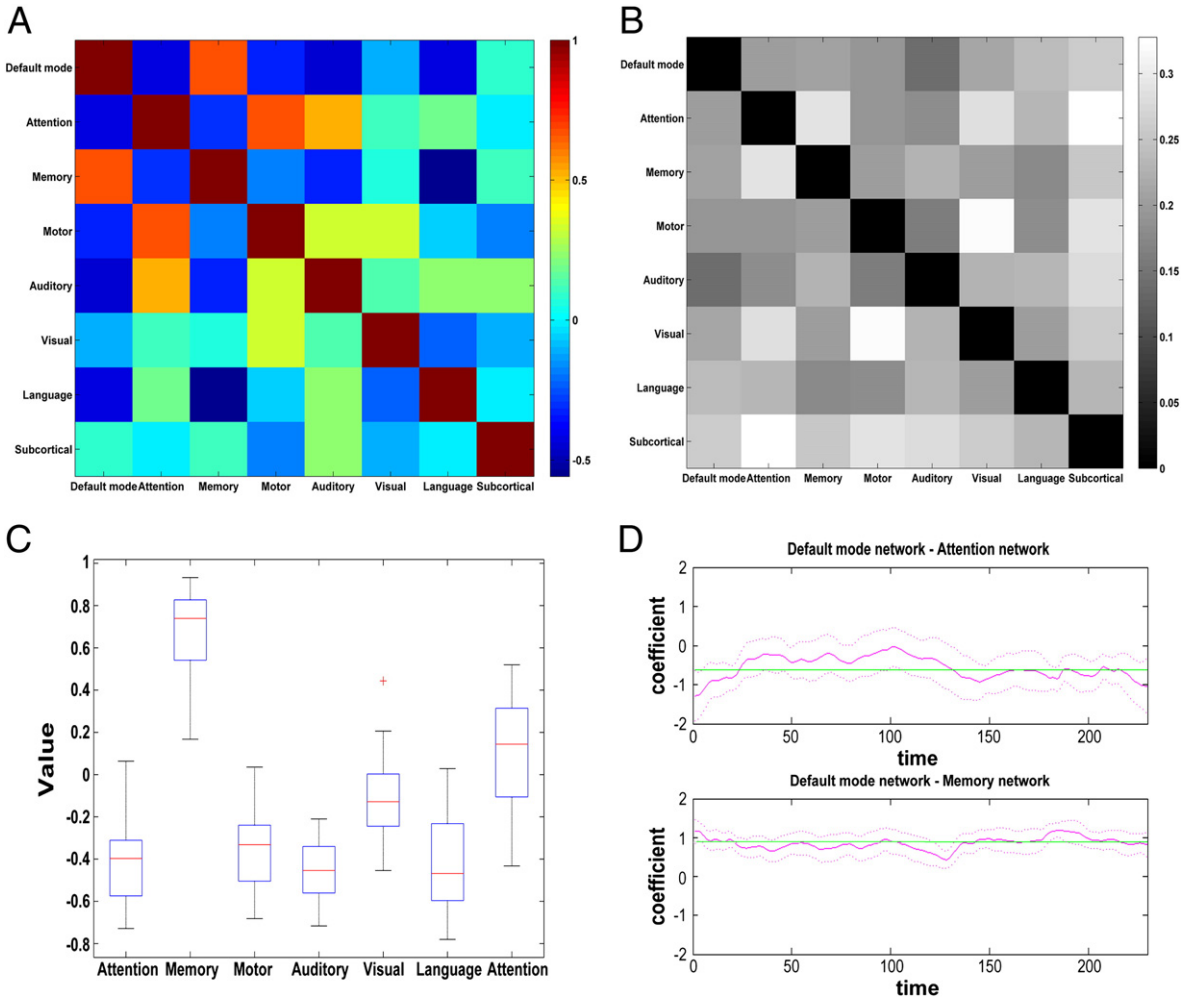

Fig. 8. The linear correlation between networks. (A) The mean of the correlation coefficients between the networks. (B) The standard deviation of correlation coefficients between the networks. (C) Default-mode network was anti-correlated with the attention, motor, auditory, visual and language networks and correlated with the memory and subcortical networks. The error bars correspond to the standard error of the mean. (D) The linear regression coefficients and the dynamic regression coefficients between the default-mode network and the attention network, and between the default-mode network and the memory network of a single subject. The green solid line denotes linear regression, the pink solid line denotes the dynamic regression and the pink dashed line denotes the standard error of the mean.

In this study, the combined VPR analysis and Kalman filtering method was employed to detect time-varying changes in functional connectivity. Other methods have been used in previous studies, such as the wavelet dynamic vector autoregressive model (Sato et al., 2006), the continuous wavelet transform (Li et al., 2007; Chang and Glover, 2010), the phase-locking value (Lachaux et al., 1999) and the sliding-window correlation (Chang and Glover, 2010). However, the wavelet dynamic vector autoregressive model and continuous wavelet transform may be compromised by the wavelet selection and edge-effects at the larger scale. Phase-locking depends on the choice of a specific frequency for analysis in order to separate the amplitude and phase components of the signals and it focuses on the detection of phase-locking between pairs recordings across trials. Windowed linear regression has poor time-resolution and be less flexible, which can be influenced by the length of window. The combined VPR analysis and Kalman filtering method used in this study could overcome these issues because (i) it is more robust and less sensitive to parameter setting, and (ii) it has a better noise suppression after smoothing. Of note, there are still some limitations of the method. First, it could not separate frequency information from the signals. Secondly, when the number of time points increases, the time of calculation will increase quickly. Thirdly, this approach does not rule out some adverse aspects such as neglected phase information (Lachaux et al., 1999; Chang and Glover, 2010). Finally, the method could not completely reflect real-time correlations because of the backward smoothing step that uses all of the late data to adjust prior estimated regression parameters.

There are some other limitations in this study. First, the low-frequency BOLD signal produced by the low frequency band-pass filtering may be insufficient to explain the spontaneous fluctuation phenomena in BOLD signals (Anderson, 2008). Although most studies have consistently identified coherently spontaneous low-frequency fluctuations in the range of 0.01–0.1 Hz during a resting state, it was difficult to accurately exclude influences of neurophysiological noises (e.g., cardiovascular and respiratory fluctuations) based on the current acquisition resolution. Second, this study revealed few strong connections between the ROI and voxels within each functional brain network. To investigate whether the stable connectivity promptly reflected anatomical connections between them, it would be interesting to utilize diffusion tensor imaging to validate this hypothesis in future studies.

Supplementary materials related to this article can be found online at doi:10.1016/j.neuroimage.2011.03.033.

Acknowledgments

We would like to thank Dr. Yufeng Zang for kindly providing the dataset. This work was supported by the National Science

Foundation of China (Nos. 81030028 and 30870667), the Beijing Natural Science Foundation (No. 7102090) and the Scientific Research Foundation for the Returned Overseas Chinese Scholars (State Education Ministry, YH).

References

Achim, A.M., Lepage, M., 2005. Dorsolateral prefrontal cortex involvement in memory post-retrieval monitoring revealed in both item and associative recognition tests. Neuroimage 24, 1113–1121.

Anderson, J.S., 2008. Origin of synchronized low-frequency blood oxygen level-dependent fluctuations in the primary visual cortex. Am. J. Neuroradiol. 29, 1722–1729.

Ashburner, J., Friston, K.J., 1999. Nonlinear spatial normalization using basis functions. Hum. Brain Mapp. 7, 254–266.

Biswal, B., Yetkin, F.Z., Haughton, V.M., Hyde, J.S., 1995. Functional connectivity in the motor cortex of resting human brain using Echo-Planar MRI. Magn. Reson. Med. 34, 537–541.

Biswal, B.B., Mennes, M., Zuo, X.N., Gohel, S., Kelly, C., Smith, S.M., Beckmann, C.F., Adelstein, J.S., Buckner, R.L., Colcombe, S., Dogonowski, A.M., Ernst, M., Fair, D., Hampson, M., Hoptman, M.J., Hyde, J.S., Kiviniemi, V.J., Kotter, R., Li, S.J., Lin, C.P., Lowe, M.J., Mackay, C., Madden, D.J., Madsen, K.H., Margulies, D.S., Mayberg, H.S., McMahon, K., Monk, C.S., Mostofsky, S.H., Nagel, B.J., Pekar, J.J., Peltier, S.J., Petersen, S.E., Riedl, V., Rombouts, S.A., Rypma, B., Schlaggar, B.L., Schmidt, S., Seidler, R.D., Siegle, G.J., Sorg, C., Teng, G.J., Veijola, J., Villringer, A., Walter, M., Wang, L., Weng, X. C., Whitfield-Gabrieli, S., Williamson, P., Windischberger, C., Zang, Y.F., Zhang, H.Y., Castellanos, F.X., Milham, M.P., 2010. Toward discovery science of human brain function. Proc. Natl. Acad. Sci. U. S. A. 107, 4734–4739.

Bressler, S.L., 1995. Large-scale cortical networks and cognition. Brain Res. Brain Res. Rev. 20, 288–304.

Buchel, C., Friston, K.J., 1998. Dynamic changes in effective connectivity characterized by variable parameter regression and Kalman filtering. Hum. Brain Mapp. 6, 403–408.

Buckner, R.L., Sepulcre, J., Talukdar, T., Krienen, F.M., Liu, H., Hedden, T., Andrews-Hanna, J.R., Sperling, R.A., Johnson, K.A., 2009. Cortical hubs revealed by intrinsic functional connectivity: mapping, assessment of stability, and relation to Alzheimer's disease. J. Neurosci. 29, 1860–1873.

Butts, C.T., 2009. Revisiting the foundations of network analysis. Science 325, 414–416.

Cabeza, R., Anderson, N.D., Houle, S., Mangels, J.A., Nyberg, L., 2000. Age-related differences in neural activity during item and temporal-order memory retrieval: a positron emission tomography study. J. Cogn. Neurosci. 12, 197–206.

Chang, C., Glover, G.H., 2010. Time–frequency dynamics of resting-state brain connectivity measured with fMRI. Neuroimage 50, 81–98.

Corbetta, M., Shulman, G.L., 2002. Control of goal-directed and stimulus-driven attention in the brain. Nat. Rev. Neurosci. 3, 201–215.

Corbetta, M., Kincade, J.M., Shulman, G.L., 2002. Neural systems for visual orienting and their relationships to spatial working memory. J. Cogn. Neurosci. 14, 508–523.

Cordes, D., Haughton, V.M., Arfanakis, K., Wendt, G.J., Turski, P.A., Moritz, C.H., Quigley, M.A., Meyerand, M.E., 2000. Mapping functionally related regions of brain with functional connectivity MR Imaging. Am. J. Neuroradiol. 21, 1636–1944.

Cordes, D., Haughton, V.M., Arfanakis, K., Carew, J.D., Turski, P.A., Moritz, C.H., Quigley, M.A., Meyerand, M.E., 2001. Frequencies contribution to functional connectivity in the cerebral cortex in “resting-state” data. Am. J. Neuroradiol. 22, 1326–1333.

Damoiseaux, J.S., Greicius, M.D., 2009. Greater than the sum of its parts: a review of studies combining structural connectivity and resting-state functional connectivity. Brain Struct. Funct. 213, 525–533.

Damoiseaux, J.S., Rombouts, S.A.R.B., Barkhof, F., Scheltens, P., Stam, C.J., Smith, S.M., Beckmann, C.F., 2006. Consistent resting-state networks across healthy subjects. Proc. Natl. Acad. Sci. U. S. A. 103, 13848–13853.

Digalakis, V., Rohlicek, J.R., 1993. ML estimation of a stochastic linear system with the EM algorithm and its application to speech recognition. IEEE Trans. Speech Audio Process. 1, 431–442.

Fox, M.D., Raichle, M.E., 2007. Spontaneous fluctuations in brain activity observed with functional magnetic resonance imaging. Nat. Rev. Neurosci. 8, 700–711.

Fox, M.D., Snyder, A.Z., Vincent, J.L., Corbetta, M., VanEssen, D.C., Raichle, M.E., 2005. The human brain is intrinsically organized into dynamic, anticorrelated functional networks. Proc. Natl. Acad. Sci. U. S. A. 102, 9673–9678.

Fox, M.D., Corbetta, M., Snyder, A.Z., Vincent, J.L., Raichle, M.E., 2006. Spontaneous neuronal activity distinguishes human dorsal and ventral attention systems. Proc. Natl. Acad. Sci. U. S. A. 103, 10046–10051.

Fox, M.D., Zhang, D., Snyder, A.Z., Raichle, M.E., 2009. The global signal and observed anticorrelated resting state brain networks. J. Neurophysiol. 101, 3270–3283.

Fransson, P., 2005. Spontaneous low-frequency BOLD signal fluctuations: an fMRI investigation of the resting-state default mode of brain function hypothesis. Hum. Brain Mapp. 26, 15–29.

Friston, K.J., Buchel, C., 2000. Attentional modulation of effective connectivity from V2 to V5/MT in humans. Proc. Natl. Acad. Sci. U. S. A. 97, 7591–7596.

Fukunaga, M., Horovitz, S.G., van Gelderen, P., de Zwart, J.A., Jansma, J.M., Ikonomidou, V.N., Chu, R., Deckers, R.H., Leopold, D.A., Duyn, J.H., 2006. Large-amplitude, spatially correlated fluctuations in BOLD fMRI signals during extended rest and early sleep stages. Magn. Reson. Imaging 24, 979–992.

Garbade, K., 1977. Two methods for examining the stability of regression coefficients. Am. Stat. Assoc. 72, 54–63.

Gautreau, A., Barrat, A., Barthelemy, M., 2009. Microdynamics in stationary complex networks. Proc. Natl. Acad. Sci. U. S. A. 106, 8847–8852.

Greicius, M.D., Krasnow, B., Reiss, A.L., Menon, V., 2003. Functional connectivity in the resting brain: a network analysis of the default mode hypothesis. Proc. Natl. Acad. Sci. U. S. A. 100, 253–258.

Greicius, M.D., Supekar, K., Menon, V., Dougherty, R.F., 2009. Resting-state functional connectivity reflects structural connectivity in the default mode network. Cereb. Cortex 19, 72–78.

Hampson, M., Peterson, B.S., Skudlarski, P., Gatenby, J.C., Gore, J.C., 2002. Detection of functional connectivity using temporal correlations in MR Images. Hum. Brain Mapp. 15, 247–262.

Harrison, B.J., Pujol, J., Ortiz, H., Fornito, A., Pantelis, C., Yucel, M., 2008. Modulation of brain resting-state networks by sad mood induction. PLoS ONE 3, e1794.

Haughton, V.M., Biswal, B., 1998. Clinical application of basal regional cerebral blood flow fluctuation measurements by FMRI. In: Hudetz, A., Bruley, D. (Eds.), Oxygen Transport to Tissue. Plenum Publishing Corp, New York, pp. 583–590.

He, Y., Wang, J., Wang, L., Chen, Z.J., Yan, C., Yang, H., Tang, H., Zhu, C., Gong, Q., Zang, Y., Evans, A.C., 2009. Uncovering intrinsic modular organization of spontaneous brain activity in humans. PLoS ONE 4, e5226.

Honey, C.J., Sporns, O., Cammoun, L., Gigandet, X., Thiran, J.P., Meuli, R., Hagmann, P., 2009. Predicting human resting-state functional connectivity from structural connectivity. Proc. Natl. Acad. Sci. U. S. A. 106, 2035–2040.

Jiang, T., He, Y., Zang, Y., Weng, X., 2004. Modulation of functional connectivity during the resting state and the motor task. Hum. Brain Mapp. 22, 63–71.

Johnston, J.M., Vaishnavi, S.N., Smyth, M.D., Zhang, D., He, B.J., Zempel, J.M., Shimony, J. S., Snyder, A.Z., Raichle, M.E., 2008. Loss of resting interhemispheric functional connectivity after complete section of the corpus callosum. J. Neurosci. 28, 6453–6458.

Kelly, A.M.C., Uddin, L.Q., Biswal, B.B., Castellanos, F.X., Milham, M.P., 2008. Competition between functional brain networks mediates behavioral variability. Neuroimage 39, 527–537.

Kellya, A.M.C., Uddina, L.Q., Biswalb, B.B., Castellanosa, F.X., Milhama, M.P., 2007. Competition between functional brain networks mediates behavioral variability. Neuroimage 39, 527–537.

Kendall, M.G., 1938. A new measure of rank correlation. Biometrika 30, 81–89.

Kiebel, S.J., Daunizeau, J., Friston, K.J., 2008. A hierarchy of time-scales and the brain. PLoS Comput. Biol. 4, e1000209.

Klaman, R.E., 1960. A new approach to linear filtering and prediction problems. Basic Eng. 82, 35–45.

Lachaux, J.P., Rodriguez, E., Martinerie, J., Varela, F.J., 1999. Measuring phase synchrony in brain signals. Hum. Brain Mapp. 8, 194–208.

Legendre, P., 2005. Species associations: the Kendall coefficient of concordance revisited. Agric. Biol. Environ. Stat. 10, 226–245.

Lewis, C.M., Baldassarre, A., Committeri, G., Romani, G.L., Corbetta, M., 2009. Learning sculpts the spontaneous activity of the resting human brain. Proc. Natl. Acad. Sci. U. S. A. 106, 17558–17563.

Li, X., Yao, X., Fox, J., Jefferys, J.G., 2007. Interaction dynamics of neuronal oscillations analysed using wavelet transforms. Neurosc. Methods 160, 178–185.

Liu, Y., Gao, J.-H., Liotti, M., Pu, Y., Fox, P.T., 1999. Temporal dissociation of parallel processing in the human subcortical outputs. Nature 400, 364–367.

Long, X.Y., Zuo, X.N., Kiviniemi, V., Yang, Y., Zou, Q.H., Zhu, C.Z., Jiang, T.Z., Yang, H., Gong, Q.Y., Wang, L., Li, K.C., Xie, S., Zang, Y.F., 2008. Default mode network as revealed with multiple methods for resting-state functional MRI analysis. J. Neurosci. Methods 171, 349–355.

Lowe, M.J., Mock, B.J., Sorenson, J.A., 1998. Functional connectivity in single and multislice echoplanar imaging using resting-state fluctuations. Neuroimage 7, 119–132.

Lowe, M.J., Dzemidzic, M., Lurito, J.T., Mathews, V.P., Phillips, M.D., 2000. Correlations in low-frequency BOLD fluctuations reflect cortico-cortical connections. Neuroimage 12, 582–587.

Majeed, W., Magnuson, M., Keilholz, S.D., 2009. Spatiotemporal dynamics of low frequency fluctuations in BOLD fMRI of the rat. J. Magn. Reson. Imaging 30, 384–393.

McGuire, P.K., Paulesu, E., Frackowiak, R.S., Frith, C.D., 1996. Brain activity during stimulus independent thought. Neuroreport 7, 2095–2099.

McKiernan, K.A., Kaufman, J.N., Kucera-Thompson, J., Binder, J.R., 2003. A parametric manipulation of factors affecting task-induced deactivation in functional neuroimaging. J. Cogn. Neurosci. 15, 394–408.

Murphy, K., Birn, R.M., Handwerker, D.A., Jones, T.B., Bandettini, P.A., 2009. The impact of global signal regression on resting state correlations: are anti-correlated networks introduced? Neuroimage 44, 893–905.

Rademacher, J., Morosan, P., Schormann, T., Schleicher, A., Werner, C., Freund, H.J., Zilles, K., 2001. Probabilistic mapping and volume measurement of human primary auditory cortex. Neuroimage 13, 669–683.

Sato, J.R., Junior, E.A., Takahashi, D.Y., MdM, Felix, Brammer, M.J., Morettin, P.A., 2006. A method to produce evolving functional connectivity maps during the course of an fMRI experiment using wavelet-based time-varying Granger causality. Neuroimage 31, 187–196.

Shehzad, Z., Kelly, A.M., Reiss, P.T., Gee, D.G., Gotimer, K., Uddin, L.Q., Lee, S.H., Margulies, D.S., Roy, A.K., Biswal, B.B., Petkova, E., Castellanos, F.X., Milham, M.P., 2009. The resting brain: unconstrained yet reliable. Cereb. Cortex 19, 2209–2229.

Shmuel, A., Leopold, D.A., 2008. Neuronal correlates of spontaneous fluctuations in fMRI signals in monkey visual cortex: implication for functional connectivity at rest. Hum. Brain Mapp. 29, 751–761.

Simpson, J.R., Ongur, D., Akbudak, E., Conturo, T.E., Ollinger, J.M., Snyder, A.Z., Gusnard, D.A., Raichle, M.E., 2000. The emotional modulation of cognitive processing: an fMRI study. J. Cogn. Neurosci. 12 (Suppl 2), 157–170.

Simpson Jr., J.R., Drevets, W.C., Snyder, A.Z., Gusnard, D.A., Raichle, M.E., 2001. Emotion-induced changes in human medial prefrontal cortex: II. During anticipatory anxiety. Proc. Natl. Acad. Sci. U. S. A. 98, 688–693.

Tian, L., Jiang, T., Liang, M., Li, X., He, Y., Wang, K., Cao, B., Jiang, T., 2007. Stabilities of negative correlations between blood oxygen level-dependent signals associated with sensory and motor cortices. Hum. Brain Mapp. 28, 681–690.

Uddin, L.Q., Kelly, A.M., Biswal, B.B., Xavier Castellanos, F., Milham, M.P., 2009. Functional connectivity of default mode network components: correlation, anticorrelation, and causality. Hum. Brain Mapp. 30, 625–637.

Valencia, M., Martinerie, J., Dupont, S., Chavez, M., 2008. Dynamic small-world behavior in functional brain networks unveiled by an event-related networks approach. Physical 77 (050905(050904)).

Vedel-Larsen, E., Fuglo, J., Channir, F., Thomsen, C.E., Sorensen, H.B., 2010. A comparative study between a simplified Kalman filter and Sliding Window Averaging for single trial dynamical estimation of event-related potentials. Comput Methods Programs Biomed 99, 252–260.

Vincent, J.L., Snyder, A.Z., Fox, M.D., Shannon, B.J., Andrews, J.R., Raichle, M.E., Buckner, R.L., 2006. Coherent spontaneous activity identifies a hippocampal-parietal memory network. J. Neurophysiol. 96, 3517–3531.

Wang, K., Jiang, T., Liang, M., Wang, L., Tian, L., Zhang, X., Li, K., Liu, Z., 2006. Discriminative analysis of early Alzheimer's disease based on two intrinsically anti-correlated networks with resting-state fMRI. Med. Image Comput. Comput. Assist. Interv. 9, 340–347.

Xiang, H.D., Fonteijn, H.M., Norris, D.G., Hagoort, P., 2010. Topographical functional connectivity pattern in the perisylvian language networks. Cereb. Cortex 20, 549–560.

Zou, Q., Wu, C.W., Stein, E.A., Zang, Y., Yang, Y., 2009a. Static and dynamic characteristics of cerebral blood flow during the resting state. Neuroimage 48, 515–524.

Zou, Q., Long, X., Zuo, X., Yan, C., Zhu, C., Yang, Y., Liu, D., He, Y., Yufeng, Zang, 2009b. Functional connectivity between the thalamus and visual cortex under eyes closed and eyes open conditions: a resting-state fMRI study. Hum. Brain Mapp. 30, 3066–3079.

Zuo, X.N., Kelly, C., Adelstein, J.S., Klein, D.F., Castellanos, F.X., Milham, M.P., 2010. Reliable intrinsic connectivity networks: test–retest evaluation using ICA and dual regression approach. Neuroimage 49, 2163–2177.